

Characterisation of an exchange-based two-qubit gate for resonant exchange qubits

Matthew P. Wardrop¹ and Andrew C. Doherty¹

¹*Centre for Engineered Quantum Systems, School of Physics,
The University of Sydney, Sydney, NSW 2006, Australia*

(Dated: 12 July 2021)

Resonant exchange qubits are a promising addition to the family of experimentally implemented encodings of single qubits using semiconductor quantum dots. We have shown previously that it ought to be straightforward to perform a CPHASE gate between two resonant exchange qubits with a single exchange pulse. This approach uses energy gaps to suppress leakage rather than conventional pulse sequences. In this paper we present analysis and simulations of our proposed two-qubit gate subject to charge and Overhauser field noise at levels observed in current experiments. Our main result is that we expect implementations of our two-qubit gate to achieve high fidelities, with errors at the percent level and gate times comparable to single-qubit operations. As such, exchange-coupled resonant exchange qubits remain an attractive approach for quantum computing.

I. INTRODUCTION

The seminal work of Loss and Divincenzo [1] introduced the notion of using individual electrons trapped in gate-defined quantum dots to encode quantum information, an idea which has since burgeoned into a family of promising architectures for quantum computing [2–12].

An early theoretical realisation was that a single qubit encoded in three electron spins could be universally controlled using exchange couplings alone [13], which removes any requirement for individually addressable electron spin resonance or magnetic field gradients. Crucially, since exchange couplings in semiconductor experiments are controllable using gate voltages, this allows all qubit operations to be performed electronically; an attractive feature in experimental implementations. Single-qubit operations for the so-called “exchange-only” qubit have been experimentally demonstrated [11, 15]. Pulse sequences are known for single-qubit gates that simultaneously correct leakage errors and other sources of noise [14]. Proposed two-qubit gates for the exchange-only qubit either involve capacitive coupling [16, 17] or exchange-coupling [13, 18–20]. Since exchange coupling is usually much larger than capacitive coupling, exchange gates are usually faster, but come at the cost of requiring complicated pulse sequences in order to echo away the unwanted spin-flip transitions that occur as a side-effect and cause leakage errors. The first such pulse sequence [13] that effected a CNOT required 19 exchange pulses in 13 timesteps, and was found using a numerical search. Since then, robust numerical searches have found improved pulse sequences that are robust against more sources of decoherence and/or reduce the number of gate operations [18–20].

A recent alternative to the “exchange-only” qubit is the “resonant-exchange qubit” [11, 21], which encodes qubits in the interaction picture with respect to significant exchange coupling between the three dots. Universal single qubit operations are effected using rf gate pulses to the electrodes controlling the exchange couplings. This qubit has been shown both theoretically [21]

and experimentally [11] to have several improved properties, including first-order insensitivity to charge fluctuations and reduced leakage error due to nuclear field fluctuations [11, 22]. In addition, Taylor et al. [21] have shown that you can perform two-qubit gates between these qubits using charge dipole interactions, while we have suggested an alternative of using simple exchange pulses between nearby qubits [23].

In this earlier work [23], we showed that a two-qubit CPHASE gate can be implemented using a single exchange pulse between the constituent quantum dots of neighbouring qubits (shown schematically in figure 2). Rapid high-fidelity gate operation is in principle made possible by energetically suppressing the spin-flip transitions that lead to leakage. This method of effecting a two-qubit gate contrasted with the more conventional approach of long and complicated pulse sequences, and is similar to our earlier proposal for singlet-triplet qubits [24].

It is the purpose of this work to extend our previous results by considering higher-order analysis, adiabatic pulse profiles, the effect of noise, and the performance of our gate in physically motivated simulations that include noise. In section II we briefly review single-qubit resonant-exchange qubit operations, in section III we review our two-qubit gates, in section IV we formally characterise our two-qubit gate in the butterfly geometry, in section V we briefly consider other geometries, and in section VI we conclude.

In this work we set $\hbar = 1$, meaning that energies are interchangeable with angular frequencies.

II. RESONANT EXCHANGE QUBITS

A resonant exchange qubit is a triple-dot system operating deep in the (1,1,1) charge state (each dot almost surely confines a single electron). A large magnetic field is applied along the z -axis, Zeeman splitting the $2^3 = 8$ spin states according to the z -projection of their total spins: $\Delta E = -m_z B_\perp$, B_\perp is the effective Zeeman splitting of an electron subject to the global magnetic

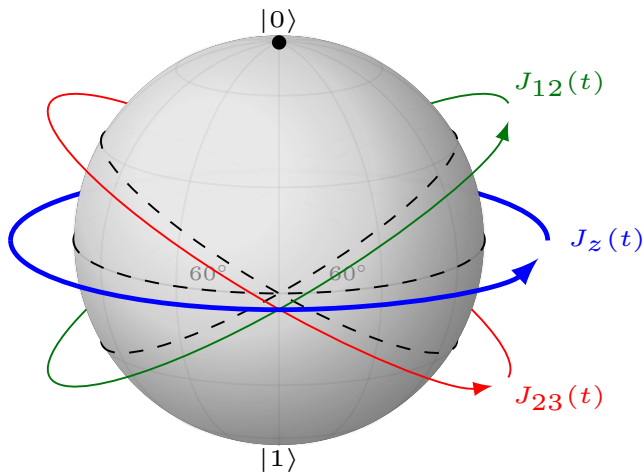


Figure 1. (colour online) A Bloch sphere schematic depicting the effect of intra-qubit exchange couplings on qubit states. Under J_{12} and J_{23} couplings, states rotate about the same axes as those of the rotations indicated in green and red respectively. If both J_{12} and J_{23} are equal to J_z , states rotate about the z axis as indicated by the emboldened blue rotation. Pulses involving different J_{12} and J_{23} couplings allow arbitrary rotations, and hence provide universal single qubit control. As these intra-qubit couplings are controllable using gate voltages, this allows for universal electronic control of qubits.

field. Note that we have absorbed the g -factor (up to its sign) into our definition of B_{\perp} . The logical states of the qubit are $|0\rangle = (|\uparrow\downarrow\rangle + |\downarrow\uparrow\rangle - 2|\uparrow\uparrow\rangle)/\sqrt{6}$ and $|1\rangle = (|\uparrow\downarrow\rangle - |\downarrow\uparrow\rangle)/\sqrt{2}$, which both have total spin $S = 1/2$ with z -projection of $m_z = 1/2$. The remainder of the eight-dimensional Hilbert space describes non-logical states, the spanning eigenstates of which are completed for the energy eigenbasis in table I. These qubits are operated with large intra-qubit exchange couplings J_{12} and J_{23} , with oscillatory modulations around $J_{12} = J_{23} = J_z$ providing single qubit control [11, 21]. This is depicted and described in more detail in figure 1. Intra-qubit exchange couplings are in turn controlled by detuning the voltages defining the quantum dots (which we parametrise as ε). This allows for complete electronic control of qubits, which potentially simplifies experimental implementation. In several GaAs singlet-triplet qubit experiments [2, 7, 9, 25], an exponential ansatz $J(\varepsilon) = J_0 \exp(\varepsilon/\varepsilon_0)$ has been found to be a good phenomenological fit to experimental data over a wide range of interesting values of ε , and so we adopt it in this work.

III. EXCHANGE-COUPLED TWO-QUBIT GATE

Here we provide a brief review of the two-qubit gate between resonant exchange qubits described in our prior letter [23]. Consider two resonant-exchange qubits (A and B) in a large transverse magnetic field, coupled in

Label	State	S	m_z	Energy
$ Q_{3/2}\rangle$	$ \uparrow\uparrow\uparrow\rangle$	3/2	3/2	$-3B_{\perp}/2$
$ 0\rangle$	$ \uparrow\uparrow\downarrow\rangle + \downarrow\uparrow\uparrow\rangle - 2 \uparrow\downarrow\uparrow\rangle$	1/2	1/2	$-B_{\perp}/2 - 3J_z/2$
$ 1\rangle$	$ \uparrow\uparrow\downarrow\rangle - \downarrow\uparrow\uparrow\rangle$	1/2	1/2	$-B_{\perp}/2 - J_z/2$
$ Q\rangle$	$ \uparrow\uparrow\downarrow\rangle + \uparrow\downarrow\uparrow\rangle + \downarrow\uparrow\uparrow\rangle$	3/2	1/2	$-B_{\perp}/2$
$ 0_{-}\rangle$	$ \downarrow\downarrow\uparrow\rangle + \uparrow\uparrow\downarrow\rangle - 2 \uparrow\downarrow\downarrow\rangle$	1/2	-1/2	$B_{\perp}/2 - 3J_z/2$
$ 1_{-}\rangle$	$ \downarrow\downarrow\uparrow\rangle - \uparrow\uparrow\downarrow\rangle$	1/2	-1/2	$B_{\perp}/2 - J_z/2$
$ Q_{-}\rangle$	$ \downarrow\downarrow\uparrow\rangle + \uparrow\downarrow\downarrow\rangle + \uparrow\uparrow\downarrow\rangle$	3/2	-1/2	$B_{\perp}/2$
$ Q_{-3/2}\rangle$	$ \downarrow\downarrow\downarrow\rangle$	3/2	-3/2	$3B_{\perp}/2$

Table I. Energy eigenstates of a single resonant exchange qubit, sorted by m_z . S is the total angular momentum quantum number of the three electron spins and m_z is the z -component of the total angular momentum. $J_z = J_{12} = J_{23}$ is the energy level splitting due to exchange coupling, and B_{\perp} is the splitting of an electron subject to the large transverse global field. Each eigenstate with a negative subscript has their constituent spins flipped relative to the corresponding unsubscripted state.

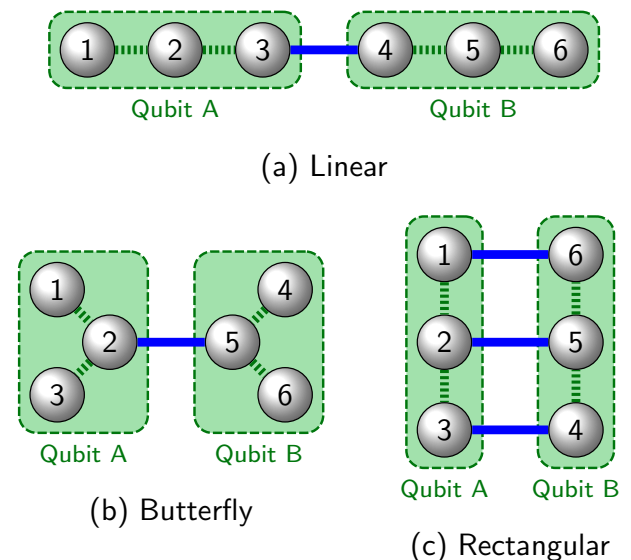


Figure 2. (colour online) The physical arrangements of quantum dots (or geometries) considered in this work. Dashed green lines indicate large intra-qubit exchange couplings, with solid blue lines indicating the weaker exchange coupling between qubits that can be used to effect two-qubit gates. We will focus mainly on the (a) butterfly and (b) linear and geometries, with the (c) rectangular geometry being another alternative.

several different ways as depicted in figure 2. We label the intra-qubit couplings of the qubits J_z^A and J_z^B , and assume that the couplings within each qubit are equal (i.e. $J_{12}^{A,B} = J_{23}^{A,B} = J_z^{A,B}$). The logical states of the two qubit system, $|0, 0\rangle$, $|0, 1\rangle$, $|1, 0\rangle$ and $|1, 1\rangle$, are all in the $m_z = 1$ subspace, along with eleven other states. Since we will only be considering dynamics which conserve z -projection of spin m_z and are working in a large global magnetic field, this reduces the dimension of the Hilbert

Geometry	$\delta J_z/J_c$	J_{zz}/J_c	J_\perp/J_c
Linear	1/36	1/36	-1/24
Butterfly	-1/18	1/9	0
Rectangular	0	1/6	-1/12

Table II. Qubit coupling parameters arising from lowest order perturbation theory in each of the three geometries of figure 2. Calculations assume that $J_z^A \simeq J_z^B$, and that all non-zero exchange couplings J_{ij} are equal to J_c . When $|J_z^B - J_z^A| \gg J_c$, the degeneracy of the logical $|10\rangle$ and $|01\rangle$ states is broken, and we find that $J_\perp \rightarrow 0$ for all geometries. All other entries in the table are unaffected.

space that can interact with the logical subspace to a maximum of 15; though in some cases (such as for the butterfly geometry) symmetry constrains this subspace further. For an explicit representation of all 15 energy levels in the energy eigenbasis, please refer to the supplementary material. The most important observation to make about the non-logical $m_z = 1$ subspace is that they all have energies different from those on the logical subspace by at least $\min(J_z^A, J_z^B, B_\perp)$. This guarantees that leakage transitions will be unfavourable provided that all additional energy-level splittings remain less than $\sim J_z$, which leads to times of order at least $\sim 1/J_z$. Since single qubit operations already run slow compared to these timescales, this is not a restriction in practice.

Using the fact that leakage processes are suppressed when $J_c \ll J_z$, we performed first order degenerate perturbation theory around $J_c = 0$ and wrote down its effect on the logical subspace; the so-called effective Hamiltonian[26] on the logical subspace. The zeroth order terms arising from perturbation theory describe the uncoupled resonant exchange qubits. Writing the Pauli-Z logical operators on qubit A and B as σ_z^A and σ_z^B respectively, the zeroth order effective Hamiltonian is:

$$H_0 = -(J_z^A + J_z^B) - \frac{1}{2}J_z^A \sigma_z^A - \frac{1}{2}J_z^B \sigma_z^B. \quad (1)$$

The first order terms describe the leading order effect of the inter-qubit coupling J_c . The effect on the logical subspace is described by:

$$H_c = \delta J_c + \frac{1}{2}\delta J_z(\sigma_z^A + \sigma_z^B) + J_{zz}\sigma_z^A\sigma_z^B + J_\perp(\sigma_x^A\sigma_x^A + \sigma_y^B\sigma_y^B), \quad (2)$$

with J_{zz} , δJ_z and J_\perp all being geometry dependent, as specified in table II. This perturbative analysis is repeated in greater detail in the supplementary material.

The structure of these effective Hamiltonians admit a straightforward two-qubit CPHASE gate using a single DC exchange pulse. Simple AC coupling pulses may also be interesting [23], but we leave this to future work. Consider first two qubits coupled according to the butterfly geometry of figure 2b. Since $J_\perp = 0$ in this geometry, the only two-qubit component of the gate's operation at first order is J_{zz} , which will implement a CPHASE gate after

a time τ such that $\int_0^\tau J_{zz} dt = \pi/4$ (modulo single qubit unitaries). The other two geometries, linear and rectangular in figures 2a and 2c respectively, have non-zero J_\perp ; and consequently will not perform a CPHASE gate unless the additional contribution can be suppressed. This can be achieved by detuning the intra-qubit exchange coupling energies such that $|J_z^B - J_z^A| \gg J_c$; or by adding a simple logical Z (σ_z^A or σ_z^B) echo pulse at $t = \tau/2$ to one of the qubits associated with each exchange coupling (which anti-commutes with $\sigma_x^A\sigma_x^B$ and $\sigma_y^A\sigma_y^B$, and thus cancels out the effect of J_\perp). We opt not to consider more sophisticated pulse sequences that echo out higher order contributions to J_\perp in order to maintain the simplicity of our gate.

IV. GATE CHARACTERISATION

We now begin a more complete characterisation of the performance of our two-qubit gate. The gate has two intrinsic sources of error (which would be present even in an ideal implementation): timing inaccuracies and leakage; and we will consider the two sources of extrinsic noise anticipated to be most pertinent in experimental implementation: charge and Overhauser noise.

In the following two subsections, we will show that intrinsic noise can be effectively mitigated by correctly tuning gate times and by adiabatic pulse sequences, resulting in high fidelity gate operations. We then move on to consider how robust our gate is to the anticipated sources of experimental noise. Simulations will be provided in each section to demonstrate the anticipated performance of our gate. These simulations involve monte-carlo averaging (over pseudo-static parameters) of solutions to a lindblad master equation (encoding high frequency noise). The performance measure used is ‘‘entanglement fidelity’’, as described in a former work [24]. ‘‘Entanglement fidelity’’ is related to the more commonly used ‘‘average fidelity’’ of random benchmarking by:

$$\bar{F} = \frac{dF_e + 1}{d + 1},$$

where \bar{F} is the average fidelity, F_e is the entanglement fidelity, and d is the dimension of the quantum system [27, 28] ($d = 4$ for our two-qubit system). Entanglement fidelity is used in this work because it can be directly computed using a fixed input state, which simplifies simulations. In this section, the simulations are usually done for the butterfly geometry which has the greatest symmetry and performance. In the next section (V), we extend our analysis to the linear geometry, which should be easier to fabricate for experiment.

A. Timing Inaccuracies

Due to the complexity of the dynamics of the six quantum dot system, there is no closed analytic form for

the ideal gate time. As a result, one needs to be careful how the gate time is estimated; over- or under-estimating the ideal gate time will result in a corresponding over or under accrual of two qubit phase, and thus reduced gate fidelities.

The ideal gate time is the time τ for which a noiseless exchange pulse should be turned on between the two triple-quantum-dot systems in order to perform a two-qubit CPHASE gate on the encoded qubits. Recall from section III that τ is implicitly defined by $\int_0^\tau J_{zz} dt = \pi/4$, with J_{zz} being geometry (and potentially time) dependent, as shown in table II.

Using the butterfly configuration as an example, first order perturbation theory predicts that $J_{zz}(J_c) = J_c/9$ and thus implies that $\tau = 9\pi \langle J_c \rangle_t / 4$; where $\langle J_c \rangle_t$ is the time average of J_c during the pulse. Note that the linearity of the first order approximation for $J_{zz}(J_c)$ allows one to compute gate time τ in a manner agnostic to the details of the pulse shape, requiring knowledge only of the average value of J_c during the pulse. This property is lost beyond first order, as $J_{zz}(J_c)$ has corrections at higher order that become significant in all geometries for physically relevant values of J_c and J_z , meaning that τ must be calibrated anew for each pulse shape.

There is no closed analytic form for τ , and since τ would in any case have to be calibrated in-situ in any experimental implementation using one of several optimisation techniques [29–32], we refer the reader to the supplementary material for a description of how we numerically optimise τ in our simulations. Henceforth, we assume τ has been estimated perfectly, and note that in many of our simulations τ differs significantly from its first order estimates.

B. Leakage

Leakage is a measure of how much a state initially with support only on the logical subspace shifts support onto the non-logical subspace during a logical operation, and results in reduced entanglement fidelities (to first non-trivial order, $\mathcal{F} = 1 - \mathcal{L}$). For an arbitrary state ρ , we quantify this using $\mathcal{L} = \text{Tr}(P\rho P)$, where $P = 1 - \sum_{l=00,01,10,11} |l\rangle \langle l|$ is the projector off the logical subspace. Leakage occurs via energetically forbidden excitations that are suppressed by the energy gap between the logical states and a leakage state, or when logical states are subjected to pulses with frequencies corresponding to the energy gap.

In the two-triple-quantum-dot system, logical states are isolated from leakage states by an energy gap ΔE proportional to J_z . When coupled using J_c , this energy gap monotonically reduces. Consequently, as the ratio J_c/J_z increases, the likelihood of leakage also increases. The energy level spectrum, with an indication as to which non-logical states the logical states can couple, is shown in figure 3. Note that the symmetries of the butterfly geometry cause J_c to couple logical states to

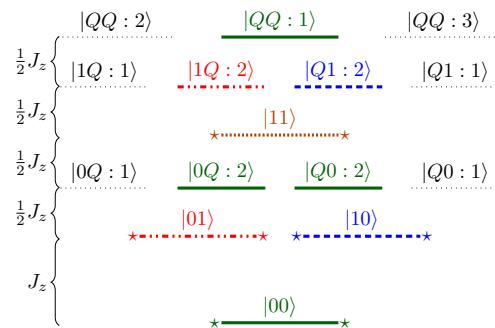


Figure 3. (colour online) The energy level spectrum of the $m_z = 1$ subspace of a two resonant exchange qubit system. Energy levels are each labelled, with starred levels indicating logical eigenstates. The eigenstates corresponding to each label are explicitly written out in the supplementary material. Under butterfly coupling J_c , the logical states couple to like coloured/dashed states leading to a minimal energy gap of $\sim 3J_z/2$. Note that the like coloured/dashed levels form distinct subspaces. Under linear coupling, all coloured/thick energy levels are coupled (including logical states), leading to a minimal energy gap of $\sim J_z/2$.

disjoint subspaces and give rise to an effective energy gap of $\Delta E = 3J_z/2$, which is three times larger than in the linear system where $\Delta E = J_z/2$ due to J_c coupling all of the logical states into the same subspace. This leads to substantially improved performance in the butterfly configuration for any given J_c/J_z .

Implementing our two-qubit gate requires J_c to be active only for a fixed duration τ , meaning that rapid or broadband changes in J_c when it is turned on and off can lead to excitations from the logical subspace. Choosing pulse shapes with discontinuities only at high differential orders can therefore further suppress leakage by several orders of magnitude, and hence improve fidelities, as shown in figure 4. For more intuition regarding adiabatic pulses and leakage refer to our earlier work on adiabatic pulses for singlet-triplet qubits [24].

In the absence of noise, the entanglement fidelity $\mathcal{F} \approx 1 - \mathcal{L}$ is limited only by leakage, which is in turn determined by the choice of adiabatic profile and the ratio J_c/J_z . This provides an upper bound on the performance of implementations of our gate. In this work, we will use a narrow-band sinusoidal adiabatic pulse described by:

$$\tilde{J}_c = J_c \left(1 - \cos \left(\frac{2\pi t}{\tau} \right) \right),$$

which has its first discontinuity at second order when $t = 0$ and τ . Note that \tilde{J}_c is chosen such that J_c is the average value of the pulse. This choice allows for fast single-pulse gates with fidelities in excess of 0.9999 for physically reasonable parameters, as shown in figure 4, and hence this gate may prove to be useful for fault-tolerant computation using semiconductor quantum dots. The remainder of this section will be devoted to determining how robust this performance is to anticipated sources of experimental noise.

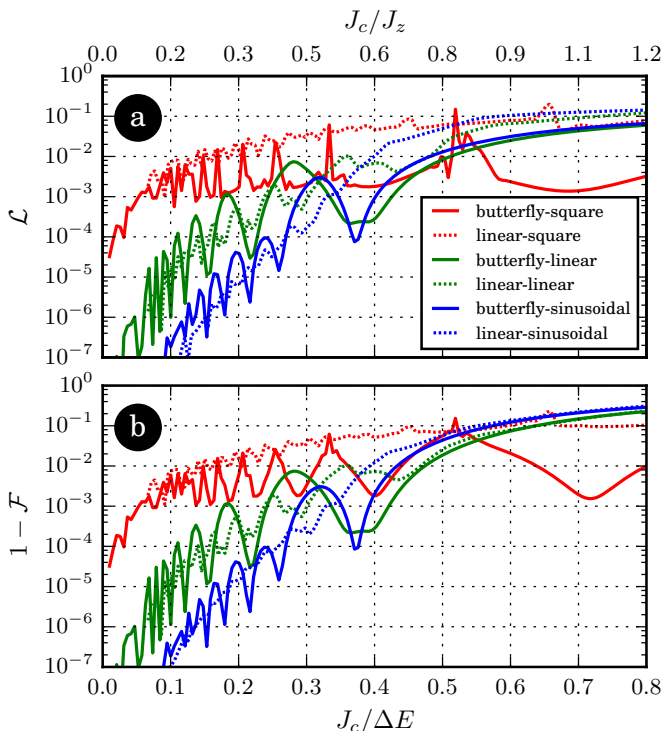


Figure 4. (colour online) (a) Leakage \mathcal{L} and (b) infidelity $1 - \mathcal{F}$ (bottom) at the end of a single two-qubit gate operation for several different adiabatic profiles in both the butterfly and linear geometries. The x-axis is shared between the plots, and is over $J_c/\Delta E$: the ratio of inter-qubit coupling and the geometry-dependent minimum energy gap. The upper x-axis provides a conversion from $J_c/\Delta E$ to J_c/J_z for the butterfly geometry (an expression in terms of the controllable parameters of the model). Colours indicate the adiabatic pulse profile used, while solid (dashed) lines denote that the butterfly (linear) geometry is being considered. Crucially, these plots demonstrate that use of adiabatic pulses can improve suppression of leakage by several orders of magnitude, provided that J_c is small compared to the energy gap; and that this leads to a corresponding increase in gate fidelities.

C. Charge Noise

One of the most significant sources of experimental noise affecting semiconductor quantum dot qubits is charge noise [11, 25]. Charge noise is the effect of fluctuations in electric potential on the gates defining the quantum dots, for which there are many causes including environmental rf radiation and Johnson noise [35]. Charge noise on the electrodes exhibits itself in our model as fluctuations in the electrode detunings ε .

In this work, we describe charge noise on ε using a two-parameter phenomenological model that approximates the noise in gate voltages by static and white noise perturbations around the desired value. The pseudo-static (DC) and white noise (HF) perturbations are respectively parameterised by the standard deviation of the pseudo-static charge offset σ_ε and the spectral density

Parameter	Value
Exchange couplings:	
$J_z = J_z^A = J_z^B$	1.65 μeV (~ 0.4 GHz)
Exponential ansatz:	
J_0	82.7 μeV (~ 20 GHz)
ε_D	0.35 mV
Charge noise:	
σ_ε	15.8 μV
D	0.244 $\mu\text{V}^2\text{ns}$
Overhauser noise:	
σ_B	2 mT

Table III. Model parameters. In the experiments of Medford et al. [11], the intra-qubit couplings J_z had measured values of roughly $0.8 \mu\text{eV}$ (0.2 GHz) to $4 \mu\text{eV}$ (1 GHz), of which we've chosen a conservative value. The parameters for the exponential ansatz $J(\varepsilon) = J_0 \exp(\varepsilon/\varepsilon_0)$ were chosen to roughly match the experimental results of Dial and collaborators [25]. The noise parameters σ_ε and D were calibrated by respectively matching somewhat typical values of $T_2^* = 25$ ns and $T_2 = 20$ μs from experiment [11, 15]. The standard deviation of the Overhauser field σ_B was chosen to be consistent with [3, 4, 33, 34].

of charge fluctuations D ; which can be respectively calibrated to experimental T_2^* and T_2 characteristic times. This is the same model described in our earlier work on singlet-triplet qubits [24], which seems to reasonably describe the results of experiments [25], even though the precise mechanisms that cause this behaviour are not perfectly understood [35]. In experiment, there are likely to be additional high-frequency T_1 processes biased toward relaxation, which we have chosen not to include in this model as it would require adding parameters to our model that have not been sufficiently well empirically constrained. Moreover, it has been found in experiment that characteristic T_1 times are in excess of $\sim 40 \mu\text{s}$ for $J_z \lesssim 1.5 \mu\text{eV}$ [11], which is long compared to T_2 times of $T_2 \sim 20 \mu\text{s}$ [11]. Even though T_1 times are found to decrease with larger J_z [11], and so at some point will become comparable to the dominant sources of noise, the performance of our gate does not appear in any case to be limited by high frequency noise in the parameter space of interest to us (see figure 5b). We therefore do not expect that the fidelity of our gate operations will be strongly affected by T_1 relaxations.

During the operation of our gate, there are multiple exchange couplings active at once (five in the case of the butterfly and linear geometries). We assume that charge noise is independent on each coupling, and use as mentioned earlier an exponential ansatz for each coupling: $J_{ij}(\varepsilon_{ij}) = J_0 \exp(\varepsilon_{ij}/\varepsilon_0)$, where i and j indicate the pair of dots being coupled. We also assume that the size and spacing of each pair of dots is the same, allowing us to use the same J_0 and ε_0 for each coupling. J_0 and ε_0 are calibrated to match such that $J(\varepsilon)$ is consistent with the data from Dial et al. [25]. In the small noise limit in which we are interested, first order analysis of the effect of perturb-

ations to the intra-qubit couplings J_{12} and J_{23} allow one to derive that $\sigma_\varepsilon = \sqrt{2}\hbar\varepsilon_0/J/T_2^*$ and $D = 2\hbar^2\varepsilon_0^2/J^2/T_2$; where J is the exchange coupling inferred from the experiment. In this work, we fit these parameters to experimental single resonant-exchange qubit T_2 times of $\sim 20\ \mu\text{s}$ and T_2^* times of $\sim 25\ \text{ns}$ [11, 15]. The resulting parameters are shown in table III.

The simplicity of the noise model and exponential ansatz allows us to construct a qualitative model from perturbation theory of the effects of this noise model on the entanglement fidelity at the end of a single two-qubit gate operation:

$$\mathcal{F} \simeq 1 - \mathcal{L} - \frac{k^2}{16\varepsilon_0^2} \left(1 + \sqrt{2}J_z^2/J_c^2\right) (\sigma_\varepsilon^2 + DJ_c/k), \quad (3)$$

where \mathcal{L} is the ultimate leakage, J_c and J_z are the inter- and intra-qubit exchange couplings respectively, ε_0 is parameter of the exponential ansatz and k is a geometry dependent constant term.

This qualitative model provides several key insights. Firstly, we learn from the $(1 + \sqrt{2}J_z^2/J_c^2)$ factor that the fidelity dimunition due to noise becomes more significant for longer gate times (J_c/J_z small), and so one is encouraged to run the gate as quickly as possible. The $\sqrt{2}J_z^2/J_c^2$ term arises from DC noise on intra-qubit couplings, and proves to be the dominant contribution to infidelity. The $(\sigma_\varepsilon^2 + DJ_c/k)$ factor suggests that DC noise (parameterised by σ_ε) leads to an approximately uniform dimunition of fidelity for any given J_c/J_z , whereas high frequency noise (parameterised by D) becomes relatively more significant as J_c increases; and that their effect is additive. Putting this all together we predict that gate performance decreases when J_c/J_z is too large (where leakage errors dominate) or too small (where low frequency charge noise dominates). For the experimentally relevant parameters considered in this work, we will not enter a regime where J_c is sufficiently large that high frequency charge noise dominates. These predictions are corroborated in simulations of the butterfly geometry including high frequency and DC charge noise, as shown in figure 5. With the noise parameters chosen to correspond to current experiments, we note that the gate's performance in the presence of charge noise appears to be limited by intra-qubit DC noise. This pseudo-static noise can in principle be echoed out by a single echo pulse. We will consider the effect of such simple echo pulses later when discussing the linear geometry. As well as echo pulses, we expect that technical developments will reduce the level of low frequency charge noise in the future.

D. Overhauser Noise

Perhaps the most widely used substrate in semiconductor quantum dot experiments is the GaAs/AlGaAs heterostructure. The nuclei in this substrate have non-zero spin, which give rise to a net magnetisation which

slowly (compared to gate times) varies due to nuclear spin flip-flop interactions [36]. This net polarisation is called an Overhauser field. While there exist semiconductor substrates composed of nuclei which do not have a spin (such as silicon and graphene), GaAs/AlGaAs has remained a popular material due to the well-developed fabrication techniques associated with it. In this section, we quantify the effect of varying levels of Overhauser noise on the performance of our gate.

The Overhauser field looks like an additional randomly oriented local magnetic field at each dot. We assume that only a small fraction of the $\sim 10^6$ nuclei in the vicinity of each dot also contribute significantly to the polarisation of an adjacent dot, and therefore make the approximation that these local fields are uncorrelated. In GaAs/AlGaAs structures, the Overhauser field has an RMS magnitude of about 1 to 3 mT [34].

We model the Overhauser field as a pseudo-static offset of the magnetic field along the z -axis sampled from a normal distribution with standard deviation σ_B . The neglected in-plane components of the random field contribute at second order in perturbation theory, and their effect is suppressed when the system is subject to a large magnetic field along z (as already posited in earlier sections), and so can be safely ignored in this analysis. For a more complete analysis, we refer the reader to Hung et al. [37].

The effect of this random Overhauser field is to couple the logical subspace to all of the fifteen $m_z = 1$ states shown in figure 3, leading to both leakage and logical errors. The logical errors directly caused by the Overhauser field are limited to single qubit errors, as must be the case since the magnetic field perturbations are local to each dot.

Simulations of entanglement fidelity for a range of different Overhauser field magnitudes in an otherwise noiseless gate implementation are shown in figure 6. Our monte-carlo simulations preferentially sample some magnetic field gradients in order to increase the rate of convergence, as described in the supplementary material. From 6a, we see that the effect of the Overhauser field is approximately linear in gate time (breaking down only once leakage becomes significant). From 6b, we see its effect is also approximately linear in the standard deviation of the field.

It should be noted that various techniques exist for reducing the magnitude of the Overhauser field in GaAs/AlGaAs, for example by nuclear state preparation which has been shown to reduce the RMS by a factor of ~ 70 [38]; in which case the effects of the Overhauser field can be largely neglected. Implementing these techniques can be quite complicated, however, and so we assume conservatively that the field will be unsuppressed .

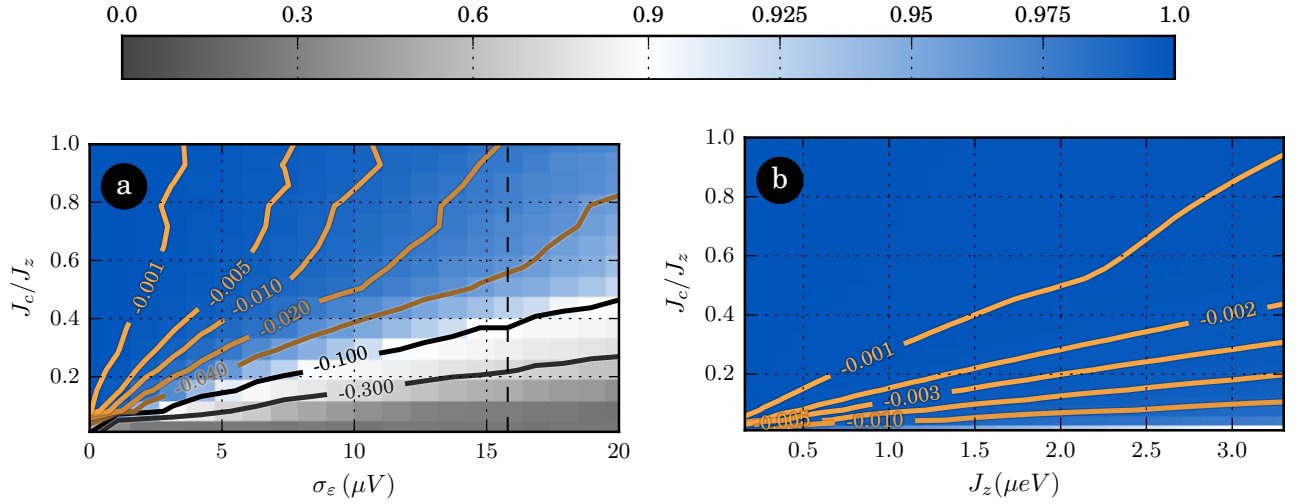


Figure 5. (colour online) The contribution to fidelity ($\mathcal{F}_{\text{noisy}} - \mathcal{F}_{\text{noiseless}}$) from (a) pseudo-static (DC) and (b) white (HF) charge noise on each of the five exchange couplings active during a single gate operation using the butterfly geometry. The colourmap used is divergent at a fidelity of 0.9, as shown above; with blue colours indicating performance in excess of 0.9, and grey colors indicating performance below 0.9. Since DC noise is essentially dependent only on the the ratio J_c/J_z , we plot in (a) the infidelity contribution as a function of J_c/J_z and σ_ϵ . The value of σ_ϵ from table III is indicated by a dashed line at $15.8 \mu\text{V}$. In (b) we plot the fidelity contribution from white charge noise for $D = 0.244 \mu\text{V}^2\text{ns}$ as in table III. The qualitative behaviour of both plots is predicted by equation 3.

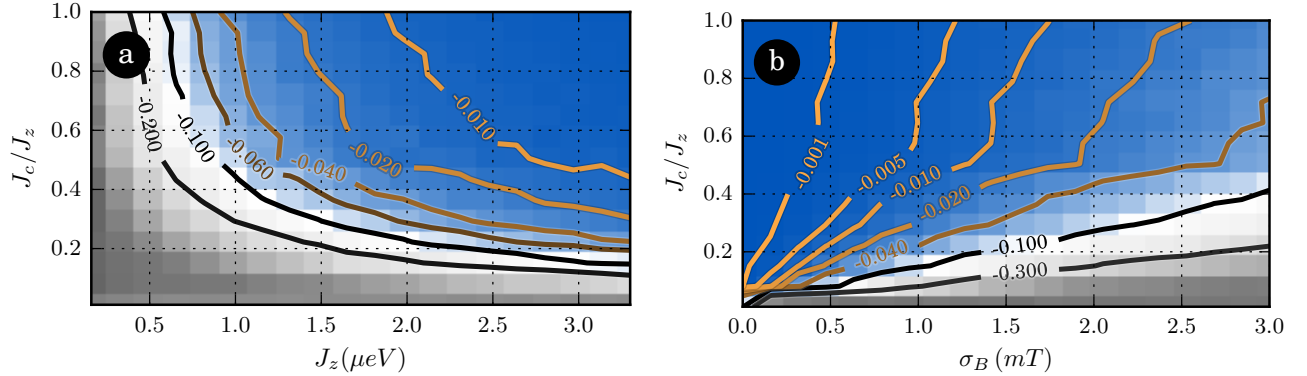


Figure 6. (colour online) The contribution to fidelity ($\mathcal{F}_{\text{noisy}} - \mathcal{F}_{\text{noiseless}}$) from a pseudo-static Overhauser field with standard deviation σ_B . In (a) the fidelity contribution is plotted as a function of J_c/J_z and J_z for $\sigma_B = 2\text{mT}$, revealing that Overhauser noise contributes to infidelity in a manner somewhat proportional to gate time (contours of constant gate time are indicated by grey lines), except at large J_c/J_z corresponding to large leakage. In (b) the fidelity contribution is plotted as a function of J_c/J_z (with fixed $J_z = 1.65 \mu\text{eV}$) and σ_B . The radial contours of (b) (in regions where leakage does not dominate) imply that infidelity is proportional to σ_B/J_c which is roughly $\propto \tau\sigma_B$, thus corroborating that the infidelity grows roughly as gate time. The colourmap used is the same as in figure 5.

E. Cumulative Noise Model

As mentioned earlier, charge and Overhauser noise are the two most significant sources of noise in semiconductor quantum dot experiments, and in this section we simulate the performance of our gate in the presence of both.

In principle the effects of Overhauser and charge noise can be more serious than for either noise source alone. For example, we learn from perturbation theory that

at second order and above, the Overhauser field cross-couples with charge noise in J_c , allowing the Overhauser field to effect genuine two-qubit errors. The larger J_c/J_z and σ_B become, the greater this cross-coupling and hence the non-linearity in the contribution of charge noise and Overhauser noise to fidelity. Fortunately, this effect is small in the parameter regime in which we are interested, and so we refer the reader to the supplementary information for more details. This is visible in the simulations

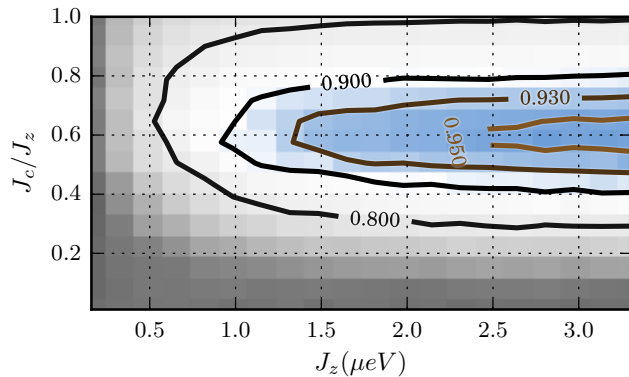


Figure 7. (colour online) Entanglement fidelity for the butterfly geometry subject to charge and Overhauser noise, as described in the main text, with noise levels calibrated to correspond to experiment (see table III). Performance is found to be limited predominantly by leakage (from above), intra-qubit DC charge noise (from below), and Overhauser noise (from the left); leading to an optimal ratio of $J_c/J_z \sim 0.6$ where fidelity reaches $\sim 95\%$ for large enough J_z . The colourmap used is the same as in figure 5.

discussed below, in which the effect of charge and Overhauser noise on gate fidelities is (very nearly) additive.

A simulation of the performance of our two-qubit gate in the presence of both charge and Overhauser noise is shown in figure 6. In this figure we see that the trade-off of avoiding leakage at large J_c/J_z , while running the gate fast enough to avoid the accumulation of DC charge noise and Overhauser noise, leads to an optimal value for J_c/J_z of approximately 0.6 for large enough J_z . Significantly, using just a single exchange pulse, we predict fidelities of ~ 0.95 with parameters currently accessible in experiment.

This optimal value of J_c/J_z is surprisingly large compared to intuitions garnered from prior arguments based on lowest order perturbation theory [23], in which one must satisfy $J_c \ll J_z$. When this tighter constraint is satisfied, implementations of this operation would actually take longer than a more traditional approach involving multiple exchange pulses [20]; and as seen in the results of our simulations, would in any case have low fidelities. That high fidelities are achievable with a large optimal value of $J_c \simeq 0.6J_z$ is one of the main results of our study, and is due to the tuning of gate times and use of adiabatic pulses discussed in sections IV A and IV B respectively.

There is still a large gap between the gate fidelities found in the presence of these realistic noise sources and the upper limit imposed by leakage, as discussed in section IV B. This could be mitigated in several ways. Firstly, one could increase our conservative choice of J_z , with larger values of J_z leading to higher fidelities; with the caveat that it has been observed in experiment that qubit relaxation rates increase with J_z , likely due to phonons. More experimental investigation would be required to determine the optimal choice of J_z , but ex-

perimental evidence [11] suggests that the parameters we have chosen are not too far from optimal for current devices. Secondly, one could add a spin echo pulse at $\tau/2$, which will be discussed in more detail for the linear geometry in the next section. For the butterfly geometry, simulations involving an echo pulse boost fidelities to ~ 0.98 at the cost of slowing down the gate. Thirdly, fidelities could be increased by suppressing the Overhauser field using DNP, or using a material without nuclear spin. We found that suppressing the Overhauser field entirely while also echoing the low frequency charge noise allowed for fidelities exceeding 0.99.

V. ALTERNATIVE GEOMETRIES

While we have so far focussed mainly on the butterfly geometry due to its simplifying symmetries and higher performance, it seems likely that it will be much easier to fabricate a linear array of quantum dots. We therefore extend our characterisation to include the anticipated performance of a linear geometry, as shown in figure 2.

In section IV B, we noted that the linear exchange coupling J_{34} lacked the symmetry of the butterfly coupling, leading to an effective energy gap three times smaller than the butterfly geometry. Figure 4 demonstrated that when this is taken into account in the absence of experimental noise, and leakage is plotted as a function of $J_c/\Delta E$, the leakage of the butterfly and linear arrangements is qualitatively similar. As detailed in section III, the J_\perp term in equation 2 is non-zero for the linear geometry, which makes it necessary to apply an echo pulse that anticommutes with the $\sigma_x^A \sigma_x^A + \sigma_y^B \sigma_y^B$ contribution at $t = 0$ and at $t = \tau/2$ in order to perform a CPHASE gate [23]. One such choice (which we adopt in this work) is a π rotation of the B qubit about the z -axis, which effects a σ_z^B operation. This could be experimentally implemented for the resonant exchange qubit by briefly shifting the value of J_{zB} . Since J_c changes the energy spectrum of the logical subspace, it is either necessary to ensure that J_c is turned off when the echo is applied. For our choice of a sinusoidal pulse envelope amounts to halving the time of the pulse and repeating it twice. Prior to each of these J_c pulses one performs the single qubit σ_{zB} operation.

The smaller energy gap ΔE means that the gate must be run more slowly than in the butterfly geometry, making the linear geometry more susceptible to noise. The most significant contribution to infidelity in figure 5a was DC noise on the intra-qubit couplings, which is geometry independent and diminishes fidelities for $J_c/J_z \lesssim 0.5$. Since leakage becomes significant in the linear geometry for $J_c/J_z \gtrsim 0.3$, without suppressing DC noise, high-fidelity operation is not possible without modifying the gate. Here we demonstrate that suppression of DC noise is possible by modifying the echo pulse used. Applying a pulse at $t = 0$ and $t = \tau/2$ that anticommutes with the

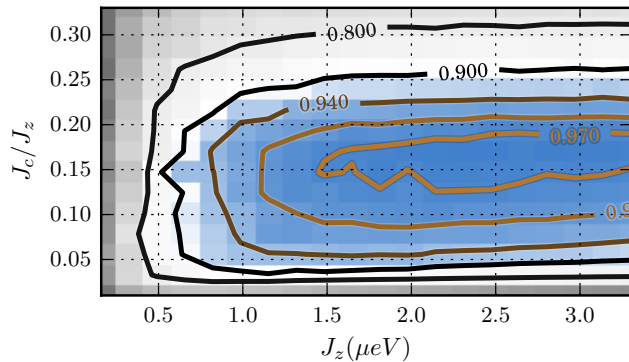


Figure 8. (colour online) Entanglement fidelity for the linear geometry subject to charge and Overhauser noise, as described in the main text, with noise levels calibrated to correspond to experiment (see table III). A single $\sigma_x^A \sigma_y^B$ echo pulse is applied at $\tau/2$ in order to echo out both intra-qubit pseudo-static charge noise and non $\sigma_z^A \sigma_z^B$ two-qubit phase, which restores maximum fidelities to $\sim 97\%$. Fidelities are limited predominantly by leakage (from above), Overhauser (from left and below), and high frequency noise (from below). The colourmap used is the same as in figure 5.

σ_z^A and σ_z^B terms of equation 1 (such as $\sigma_x^A \sigma_x^B$) will echo out the effect of DC noise on the intra-qubit couplings. This can be merged with the σ_z^B pulse discussed above. In this work we choose to apply a $\sigma_x^A \sigma_x^B$ pulse, which becomes (up to irrelevant phase) $\sigma_x^A \sigma_y^B$ when merged with σ_z^B . Note that this amounts to an independent simultaneous π rotation for each qubit. In resonant exchange qubits this pulse can be achieved by oscillatory J pulses that are chosen to be out of phase by $\pi/2$. In the simulations shown in figure 8 we demonstrate that these pulse sequences result in improved fidelities of $\sim 97\%$.

Similar to the butterfly geometry, gate performance is reduced for large and small values of J_c/J_z by leakage and (inter-qubit) DC charge noise respectively; and for small values of J_z and/or J_c/J_z by Overhauser noise.

In this analysis, we have assumed that the echo pulses (which are single qubit operations) are instantaneous and performed with higher fidelity than two-qubit operations. In actual fact, current experiments demonstrate single qubit gate times several times longer [11] than the duration of our two-qubit gate. At this preliminary stage, however, single qubit operations gate times have not been optimised, and we expect single qubit gate times could be reduced to a point where they are not limiting gate performance. In any case, our primary objective is to show that two-qubit gate operations in semiconductor systems can be implemented with times and fidelities comparable to single qubit operations, and so we have left a more detailed study to future work.

VI. DISCUSSION

In this paper we have extended the analysis of our proposal for a two-qubit CPHASE gate between resonant-exchange qubits [23], which uses the large intra-qubit exchange couplings to energetically suppress leakage caused by inter-qubit exchange couplings. In particular, we have: demonstrated that high-fidelity two-qubit operations are possible with gate times comparable to single-qubit operations, provided that gate times are carefully tuned to account for perturbations beyond first order; demonstrated that leakage can be further suppressed by using adiabatic pulse profiles; and shown in conservative simulations that the infidelities of our two-qubit gate are small (a few percent) even when subject to charge and Overhauser noise that has been calibrated to recent experiment.

Our two-qubit gate works whenever there is an effective exchange coupling between the qubits. This could be a direct exchange coupling (as we have envisaged here), or an indirect coupling through an intermediate dot which has recently been shown to generate an effective exchange interaction [39, 40].

In our analysis, we found (intra-qubit) DC charge noise on the electrodes defining the quantum dots to be the most potent source of gate infidelity. While we have chosen our noise parameters to match experimental results, we do not believe there is any fundamental reason why this noise cannot be substantially reduced. The next largest source of infidelity was the Overhauser field. We calibrated our simulations to reflect an unsuppressed Overhauser field in GaAs/AlGaAs heterostructures. It is possible to suppress the Overhauser field fluctuations using dynamic nuclear polarisation [41–43], which can reduce the standard deviation of the field fluctuations by several orders of magnitude (e.g. [38]). It seems reasonable to expect that our two-qubit gate’s fidelities may exceed 99% even without using echo pulses. Of course, since low-frequency (DC) noise and the Overhauser field fluctuations vary very slowly compared to gate times, it should be reasonably simple to use echo pulses or dynamical decoupling if necessary.

A surprising result, perhaps, is that optimal ratio of inter-qubit coupling to intra-qubit coupling J_c/J_z is actually quite large, especially in the butterfly geometry. As a consequence, it is not necessary to run these gates particularly slowly, allowing our gate to run faster (and possibly with greater fidelity) than even the most carefully constructed pulse sequences (e.g. [20]).

Our approach of energetically suppressing spin-flip transitions in order to implement two-qubit gates using exchange coupling has utility in other qubit architectures, as we have already shown in singlet-triplet qubits [24]. The main benefit of this approach is to remove dependence on complicated pulse-sequences in order to achieve high fidelities.

The relative simplicity of our two qubit gate, coupled with its high performance, commends it for implementa-

tion in contemporary experiment.

ACKNOWLEDGMENTS

We acknowledge helpful conversations with Charles Marcus. Research was supported by the Office of the Dir-

ector of National Intelligence, Intelligence Advanced Research Projects Activity (IARPA), through the Army Research Office grant W911NF-12-1-0354 and by the Australian Research Council (ARC) via the Centre of Excellence in Engineered Quantum Systems (EQuS), project number CE110001013.

-
- [1] D. Loss and D. P. DiVincenzo, *Physical Review A* **57**, 120 (1998).
- [2] J. R. Petta, A. C. Johnson, J. M. Taylor, E. A. Laird, A. Yacoby, M. D. Lukin, C. M. Marcus, M. P. Hanson, and A. C. Gossard, *Science* **309**, 2180 (2005).
- [3] F. H. L. Koppens, C. Buizert, K. J. Tielrooij, I. T. Vink, K. C. Nowack, T. Meunier, L. P. Kouwenhoven, and L. M. K. Vandersypen, *Nature* **442**, 766 (2006).
- [4] K. C. Nowack, F. H. L. Koppens, Y. V. Nazarov, and L. M. K. Vandersypen, *Science (New York, N.Y.)* **318**, 1430 (2007).
- [5] M. Pioro-Ladrière, T. Obata, Y. Tokura, Y.-S. Shin, T. Kubo, K. Yoshida, T. Taniyama, and S. Tarucha, *Nature Physics* **4**, 776 (2008).
- [6] C. Barthel, D. Reilly, C. Marcus, M. Hanson, and A. Gossard, *Physical Review Letters* **103**, 160503 (2009).
- [7] S. Foletti, H. Bluhm, D. Mahalu, V. Umansky, and A. Yacoby, *Nature Physics* **5**, 903 (2009).
- [8] M. D. Shulman, O. E. Dial, S. P. Harvey, H. Bluhm, V. Umansky, and A. Yacoby, *Physics* **1**, 202 (2012), arXiv:1202.1828.
- [9] E. A. Laird, J. M. Taylor, D. P. DiVincenzo, C. M. Marcus, M. P. Hanson, and A. C. Gossard, *Physical Review B* **82**, 075403 (2010).
- [10] L. Gaudreau, G. Granger, A. Kam, G. C. Aers, S. A. Studenikin, P. Zawadzki, M. Pioro-Ladrière, Z. R. Wasilewski, and A. S. Sachrajda, *Nature Physics* **8**, 54 (2012).
- [11] J. Medford, J. Beil, J. M. Taylor, E. I. Rashba, H. Lu, A. C. Gossard, and C. M. Marcus, *Physical Review Letters* **111**, 050501 (2013).
- [12] C. Kloeffel and D. Loss, *Annual Review of Condensed Matter Physics* **4**, 51 (2013).
- [13] D. P. DiVincenzo, D. Bacon, J. Kempe, G. Burkard, and K. B. Whaley, *Nature* **408**, 339 (2000), arXiv:0005116v2 [arXiv:quant-ph].
- [14] G. T. Hickman, X. Wang, J. P. Kestner, and S. Das Sarma, *Physical Review B - Condensed Matter and Materials Physics* **88**, 1 (2013).
- [15] J. Medford, J. Beil, J. M. Taylor, S. D. Bartlett, A. C. Doherty, E. I. Rashba, D. P. DiVincenzo, H. Lu, A. C. Gossard, and C. M. Marcus, *Nature nanotechnology* **8**, 654 (2013).
- [16] A. Pal, E. I. Rashba, and B. I. Halperin, arXiv preprint 1505.07847 (2015).
- [17] A. Pal, E. I. Rashba, and B. I. Halperin, *Physical Review X* **4**, 1 (2014).
- [18] Y. Kawano, K. Kimura, H. Sekigawa, M. Noro, K. Shirayanagi, M. Kitagawa, and M. Ozawa, *Quantum Information Processing* **4**, 65 (2005).
- [19] B. H. Fong and S. M. Wandzura, *Quantum Info. Comput.* **11**, 1003 (2011).
- [20] F. Setiawan, H. Y. Hui, J. P. Kestner, X. Wang, and S. D. Sarma, *Physical Review B - Condensed Matter and Materials Physics* **89**, 1 (2014).
- [21] J. M. Taylor, V. Srinivasa, and J. Medford, *Physical Review Letters* **111**, 050502 (2013).
- [22] J. Fei, J.-t. Hung, T. S. Koh, Y.-p. Shim, S. N. Copper-smith, X. Hu, and M. Friesen, *Physical Review B* **91**, 205434 (2015).
- [23] A. C. Doherty and M. P. Wardrop, *Physical review letters* **111**, 050503 (2013), arXiv:1304.3416.
- [24] M. P. Wardrop and A. C. Doherty, *Physical Review B* **90**, 045418 (2014).
- [25] O. Dial, M. Shulman, S. Harvey, H. Bluhm, V. Umansky, and A. Yacoby, *Physical Review Letters* **110**, 146804 (2013).
- [26] C. Cohen-Tannoudji, J. Dupont-Roc, and G. Grynberg, in *Atom-Photon Interactions* (Wiley-VCH Verlag GmbH, Weinheim, Germany, 2008) pp. 5–66.
- [27] M. Horodecki, P. Horodecki, and R. Horodecki, *Physical Review A* **60**, 1888 (1999).
- [28] M. A. Nielsen, *Physics Letters A* **303**, 249 (2002).
- [29] J. Kelly, R. Barends, B. Campbell, Y. Chen, Z. Chen, B. Chiaro, A. Dunsworth, a. G. Fowler, I. C. Hoi, E. Jeffrey, A. Megrant, J. Mutus, C. Neill, P. J. J. O’Malley, C. Quintana, P. Roushan, D. Sank, A. Vainsencher, J. Wenner, T. C. White, a. N. Cleland, and J. M. Martinis, *Physical Review Letters* **112**, 1 (2014).
- [30] D. J. Egger and F. K. Wilhelm, *Physical Review Letters* **112**, 1 (2014).
- [31] C. Ferrie and O. Moussa, *Physical Review A* **91**, 052306 (2015).
- [32] C. E. Granade, *Characterization, Verification and Control for Large Quantum Systems*, Ph.D. thesis, University of Waterloo, Ontario, Canada (2014).
- [33] F. H. L. Koppens, C. Buizert, I. T. Vink, K. C. Nowack, T. Meunier, L. P. Kouwenhoven, and L. M. K. Vandersypen, *Journal of Applied Physics* **101** (2007), 10.1063/1.2722734.
- [34] D. J. Reilly, J. M. Taylor, E. a. Laird, J. R. Petta, C. M. Marcus, M. P. Hanson, and a. C. Gossard, *Physical Review Letters* **101**, 1 (2008).
- [35] F. Beaudoin and W. A. Coish, *Physical Review B* **91**, 165432 (2015).
- [36] J. M. Taylor, J. R. Petta, A. C. Johnson, A. Yacoby, C. M. Marcus, and M. D. Lukin, *Physical Review B* **76**, 035315 (2007).
- [37] J. T. Hung, J. Fei, M. Friesen, and X. Hu, *Physical Review B - Condensed Matter and Materials Physics* **90**, 1 (2014).
- [38] D. J. Reilly, J. M. Taylor, J. R. Petta, C. M. Marcus, M. P. Hanson, and A. C. Gossard, *Science (New York, N.Y.)* **321**, 817 (2008).

- [39] F. Braakman, P. Barthelemy, C. Reichl, W. Wegschneider, and V. L.M.K., *Nature nanotechnology* **8**, 432 (2013).
- [40] S. Mehl, H. Bluhm, and D. P. DiVincenzo, *Physical Review B* **90**, 045404 (2014), arXiv:1403.2910.
- [41] A. Brataas and E. I. Rashba, *Physical Review B* **89**, 035423 (2014).
- [42] I. Neder, M. S. Rudner, and B. I. Halperin, *Physical Review B* **89**, 085403 (2014).
- [43] J. M. Nichol, S. P. Harvey, M. D. Shulman, A. Pal, V. Umansky, E. I. Rashba, B. I. Halperin, and A. Yacoby, arXiv preprint 1502.05400 (2015).

Supplementary A: Energy eigenstates for the $m_z = 1$ subspace

In this section we list the energy eigenstates for the $m_z = 1$ subspace of the two resonant-exchange qubit system, in terms of the single qubit states listed in table I of the main text. Where an energy degeneracy occurs, we choose states that maximally exploit the symmetries of the butterfly geometry, in order to reproduce the splitting and coupling shown in figure 3 of the main text. In particular, the states of the butterfly configuration are invariant under global spin rotations, allowing one to write the degenerate subspace in terms of states with definite angular momentum using standard Clebsch-Gordan coefficients. The states, along with their symmetries, are listed in the following table, in eigenstates are sorted by energy and then by total angular momentum S . Note that energies omit the constant $-B_\perp$ contribution shared by all states. The eigenstate label is chosen to indicate which elements of the single subspace are involved, and then append a colon followed by the total angular momentum (with the exception of logical states, where the total angular momentum is omitted). The ‘‘Parity’’ column indicates the parity accumulated by the state under the operation involving swapping dot 1 and 3 (the first sign) and 4 and 6 (the second sign) in the butterfly geometry. $+-$, for example, indicates that the state is unchanged under swapping the dots in the first qubit, but attracts a negative sign when swapping the dots of the second. The ‘‘Swap’’ column indicates the parity of the state when interchanging the qubits, where this is well-defined. Horizontal lines form the states into groups of equal energy.

Label	State	Energy ($+B_\perp$)	S	Parity	Swap
$ QQ : 1\rangle$	$\sqrt{\frac{2}{5}} Q, Q\rangle - \sqrt{\frac{3}{10}} (Q_{3/2}, Q_-\rangle + Q_-, Q_{3/2}\rangle)$	0	1	++	+
$ QQ : 2\rangle$	$\sqrt{\frac{1}{5}} (Q_{3/2}, Q_-\rangle - Q_-, Q_{3/2}\rangle)$	0	2	++	-
$ QQ : 3\rangle$	$\sqrt{\frac{3}{5}} Q, Q\rangle + \sqrt{\frac{1}{5}} (Q_{3/2}, Q_-\rangle + Q_-, Q_{3/2}\rangle)$	0	3	++	+
$ 1Q : 1\rangle$	$\frac{1}{2} 1, Q\rangle - \frac{\sqrt{3}}{2} 1_-, Q_{3/2}\rangle$	$-\frac{1}{2} J_z^A$	1	--	
$ 1Q : 2\rangle$	$\frac{\sqrt{3}}{2} 1, Q\rangle + \frac{1}{2} 1_-, Q_{3/2}\rangle$	$-\frac{1}{2} J_z^A$	2	--	
$ Q1 : 1\rangle$	$\frac{1}{2} Q, 1\rangle - \frac{\sqrt{3}}{2} Q_{3/2}, 1_-\rangle$	$-\frac{1}{2} J_z^B$	1	+-	
$ Q1 : 2\rangle$	$\frac{\sqrt{3}}{2} Q, 1\rangle + \frac{1}{2} Q_{3/2}, 1_-\rangle$	$-\frac{1}{2} J_z^B$	2	+-	
$ 11\rangle$	$ 1, 1\rangle$	$-\frac{1}{2} (J_z^A + J_z^B)$	1	--	+
$ 0Q : 1\rangle$	$\frac{1}{2} 0, Q\rangle - \frac{\sqrt{3}}{2} 0_-, Q_{3/2}\rangle$	$-\frac{3}{2} J_z^A$	1	++	
$ 0Q : 2\rangle$	$\frac{\sqrt{3}}{2} 0, Q\rangle + \frac{1}{2} 0_-, Q_{3/2}\rangle$	$-\frac{3}{2} J_z^A$	2	++	
$ Q0 : 1\rangle$	$\frac{1}{2} Q, 0\rangle - \frac{\sqrt{3}}{2} Q_{3/2}, 0_-\rangle$	$-\frac{3}{2} J_z^B$	1	++	
$ Q0 : 2\rangle$	$\frac{\sqrt{3}}{2} Q, 0\rangle + \frac{1}{2} Q_{3/2}, 0_-\rangle$	$-\frac{3}{2} J_z^B$	2	++	
$ 10\rangle$	$ 1, 0\rangle$	$\frac{1}{2} (J_z^A + 3J_z^B)$	1	--	
$ 01\rangle$	$ 0, 1\rangle$	$\frac{1}{2} (3J_z^A + J_z^B)$	1	+-	
$ 00\rangle$	$ 0, 0\rangle$	$\frac{3}{2} (J_z^A + J_z^B)$	1	++	+

Supplementary B: Derivation of the Effective Hamiltonian

In this section we describe how the effective Hamiltonian of equations 1 and 2 in the main text is lifted from perturbation theory, the procedure for which follows standard practice [26]. The main idea is that, in the limit that inter-qubit coupling J_c is small compared to intra-qubit coupling J_z , the evolution of the logical subspace in which we are interested should be well-approximated by low-order terms in a perturbation expansion around $J_c = 0$; from which considerable insight might be gained into qubit dynamics.

To generate the effective Hamiltonian for a given geometry, we perturb the Hamiltonian describing the two decoupled resonant exchange qubits with the Hamiltonian describing the two-qubit coupling of that geometry, to first order in a Rayleigh-Schrodinger perturbation expansion. We then construct the effective Hamiltonian using the resulting energies E and eigenvectors $|E\rangle$ that adiabatically map to the logical states using $H_{\text{eff}} = \sum_E E |E\rangle \langle E|$. This algorithm explicitly disregards any leakage operations, but captures the dominant dynamics on the logical subspace. The result is a diagonal Hamiltonian, except where the original logical states were degenerate.

For our two resonant exchange qubit system, in which the $|01\rangle$ and $|10\rangle$ states are degenerate (shown in figure 3 of the main text), this results in a block-diagonal Hamiltonian when written in the basis $\{|00\rangle, |01\rangle, |10\rangle, |11\rangle\}$. We

explicitly compute the effective Hamiltonians for the geometries shown in figure 2 of the main text; that is, the linear, butterfly and rectangular geometries respectively. We also explicitly compute the coefficients of $\sigma_I^A \sigma_I^B$, $\sigma_x^A \sigma_x^B$, $\sigma_y^A \sigma_y^B$, and $\sigma_z^A \sigma_z^B$, which are then used to populate table II of the main text.

1. Linear

$$H_{\text{eff}} = \begin{bmatrix} -\frac{5J_{34}}{36} - \frac{3J_z^A}{2} - \frac{3J_z^B}{2} & 0 & 0 & 0 \\ 0 & -\frac{J_{34}}{4} - \frac{3J_z^A}{2} - \frac{J_z^B}{2} & -\frac{J_{34}}{12} & 0 \\ 0 & -\frac{J_{34}}{12} & -\frac{J_{34}}{4} - \frac{J_z^A}{2} - \frac{3J_z^B}{2} & 0 \\ 0 & 0 & 0 & -\frac{J_{34}}{4} - \frac{J_z^A}{2} - \frac{J_z^B}{2} \end{bmatrix}$$

$$\text{coefficients} = \begin{bmatrix} -\frac{2J_{34}}{9} - J_z^A - J_z^B \\ \frac{J_{34}}{36} - \frac{J_z^B}{2} \\ \frac{J_{34}}{36} - \frac{J_z^A}{2} \\ \frac{J_{34}}{36} \end{bmatrix}$$

2. Butterfly

$$H_{\text{eff}} = \begin{bmatrix} -\frac{2J_{25}}{9} - \frac{3J_z^A}{2} - \frac{3J_z^B}{2} & 0 & 0 & 0 \\ 0 & -\frac{J_{25}}{3} - \frac{3J_z^A}{2} - \frac{J_z^B}{2} & 0 & 0 \\ 0 & 0 & -\frac{J_{25}}{3} - \frac{J_z^A}{2} - \frac{3J_z^B}{2} & 0 \\ 0 & 0 & 0 & -\frac{J_z^A}{2} - \frac{J_z^B}{2} \end{bmatrix}$$

$$\text{coefficients} = \begin{bmatrix} -\frac{2J_{25}}{9} - J_z^A - J_z^B \\ -\frac{J_{25}}{18} - \frac{J_z^B}{2} \\ -\frac{J_{25}}{18} - \frac{J_z^A}{2} \\ \frac{J_{25}}{9} \end{bmatrix}$$

3. Rectangular

$$H_{\text{eff}} = \begin{bmatrix} -\frac{5J_{16}}{36} - \frac{2J_{25}}{9} - \frac{5J_{34}}{36} - \frac{3J_z^A}{2} - \frac{3J_z^B}{2} & 0 & 0 & 0 \\ 0 & -\frac{J_{16}}{4} - \frac{J_{25}}{3} - \frac{J_{34}}{4} - \frac{3J_z^A}{2} - \frac{J_z^B}{2} & -\frac{J_{16}}{12} - \frac{J_{34}}{12} & 0 \\ 0 & -\frac{J_{16}}{12} - \frac{J_{34}}{12} & -\frac{J_{16}}{4} - \frac{J_{25}}{3} - \frac{J_{34}}{4} - \frac{J_z^A}{2} - \frac{3J_z^B}{2} & 0 \\ 0 & 0 & 0 & -\frac{J_{16}}{4} - \frac{J_{34}}{4} - \frac{J_z^A}{2} - \frac{J_z^B}{2} \end{bmatrix}$$

$$\text{coefficients} = \begin{bmatrix} -\frac{2J_{16}}{9} - \frac{2J_{25}}{9} - \frac{2J_{34}}{9} - J_z^A - J_z^B \\ \frac{J_{16}}{36} - \frac{J_{25}}{18} + \frac{J_{34}}{36} - \frac{J_z^B}{2} \\ \frac{J_{16}}{36} - \frac{J_{25}}{18} + \frac{J_{34}}{36} - \frac{J_z^A}{2} \\ \frac{J_{16}}{36} + \frac{J_{25}}{9} + \frac{J_{34}}{36} \end{bmatrix}$$

Note that to recover the provided coefficients in table II of the main text, we assume that all inter-qubit couplings (J_{16} , J_{25} and J_{34}) are equal to J_c .

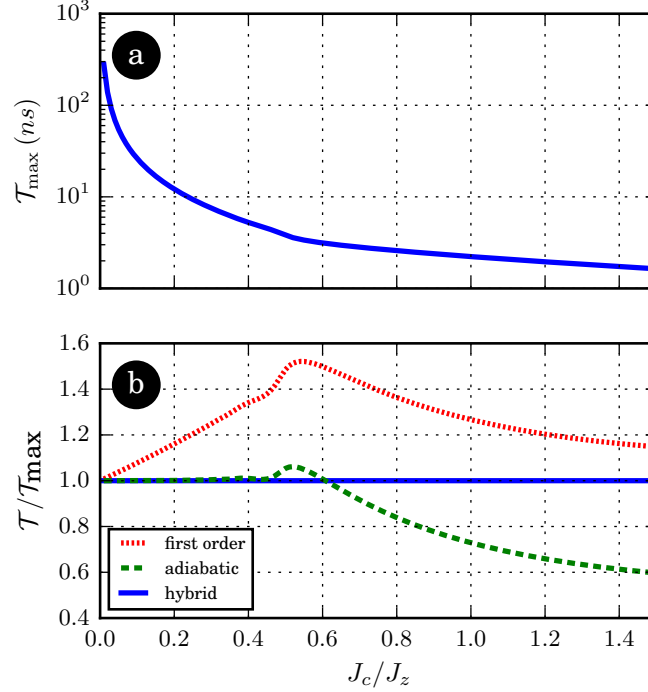


Figure 9. (colour online) In (a) we plot the ideal gate time \mathcal{T}_{\max} as computed using the “hybrid” method described in the text, which is our best approach for maximising the fidelity of gate operations. $\mathcal{T}_{\max}(J_c/J_z)$ is defined as in the text, and plotted here for $J_z^{\text{ref}} = 1.65 \mu\text{eV}$. In (b) we plot the relative difference $\mathcal{T}/\mathcal{T}_{\max}$ of the other methods described in the text, namely “adiabatic” (green dashed) and “first order” (red dotted) methods, to the “hybrid” estimate (blue solid). The plots share the same x axis, which is the ratio of intra-qubit coupling to inter-qubit coupling J_c/J_z . Note that the first order approximation consistently underestimates the phase accrual rate, and so overestimates the gate time. While an adiabatic phase estimation does better, it ends up underestimating the phase due to the importance of evolution off the logical subspace for large enough J_c .

Supplementary C: Estimating Ideal Gate Time

As mentioned in section IVA, over- or under-estimating the ideal gate time τ leads to over- or under-accrual of two-qubit phase, resulting in poor gate fidelities. In particular, using a first order approximation neglects higher order terms that give rise to convex non-linearity in $J_{zz}(J_c)$, and so consistently exaggerates gate times. In this section, we describe the method by which we obtain accurate timing estimates for use in the simulations of the main text.

There are two methods that one might employ to find an estimate of τ that includes high order perturbations. One can make the assumption that evolution is perfectly adiabatic, solve for the eigenvalues at different values of inter-qubit coupling J_c , and thus infer the two-qubit phase accumulation rate J_{zz} ; or, alternatively, one can locally maximise the gate fidelity over gate times. The first method works well for small values of J_c/J_z (where the adiabatic approximation make sense), and the second method works well for larger values of J_c/J_z (where gate times are shorter, and numerical integration has less time to accumulate error). We therefore use a hybrid approach that works well across all values of J_c/J_z : for $J_c/J_z \leq 0.15$, we use the adiabatic approach, and for $J_c/J_z > 0.15$ we use the adiabatic approach to seed a numerical optimisation of gate fidelity over gate times.

As noted in the main text, the non-linearity of $J_{zz}(J_c)$ means that we must repeat this estimation process for each pulse shape considered. As the dynamics of our (noiseless) two-qubit system is determined by the ratio of J_c/J_z , given a particular pulse shape, we need only optimise over the ratio of the two physical degrees of freedom, rather than both. We therefore proxy the optimisation of $\tau(J_c, J_z)$ for any given pulse shape by optimisations over the single parameter function $\mathcal{T}(J_c/J_z)$. In practice we fix a value of $J_z = J_z^{\text{ref}}$, and vary J_c . τ can be recovered from \mathcal{T} using:

$$\tau(J_c, J_z) = \frac{J_z^{\text{ref}}}{J_z} \mathcal{T}(J_c/J_z).$$

The gate time for maximum fidelity \mathcal{T}_{\max} for the butterfly configuration using a sinusoidal adiabatic pulse profile is shown in figure 9, along with the relative error of the first order and adiabatic estimations. We note that the first

order approximation consistently underestimates the phase accrual rate, and so overestimates the gate time. While an adiabatic phase estimation does better at first, it ends up underestimating the phase due to the importance of evolution off the logical subspace for large enough J_c .

Supplementary D: Accelerating Monte-Carlo Convergence in Overhauser Simulations

Simulations involving the Overhauser field modelled as described in the main text requires averaging over a multivariate normal distribution in 6 variables (11 if DC charge noise is also considered). While a naive Monte-Carlo simulation that samples the local Overhauser field contribution for each dot will converge eventually, we speed up the convergence by instead sampling preferentially from linear combinations of local Overhauser contributions that appear at lower order in perturbation theory.

Inspired by perturbation theory, we form a spanning basis for the magnetic fields:

$$\begin{aligned} B_0 &= \frac{1}{6} \sum_n B_n \\ \Delta B &= \frac{1}{3} \left(\sum_{n \leq 3} B_n - \sum_{n \geq 4} B_n \right) \\ \Delta_{ij} &= B_i - B_j \text{ for } \Delta_{13} \text{ and } \Delta_{46} \\ \Delta_{ijk} &= B_i - 2B_j + B_k \text{ for } \Delta_{123} \text{ and } \Delta_{456} \end{aligned}$$

where B_n (with $n \in [1, 6]$) is the z-component of the Overhauser field at dot n . We learn from perturbation theory that Δ_{123} and Δ_{456} first contribute at zeroth order in perturbation theory, Δ_{13} and Δ_{46} at first order, and ΔB at fourth order. As B_0 is a global field, it does not contribute.

The higher the order at which the terms contribute, the more significant that term is to the dynamics of the qubit system. It makes sense, therefore, to sample lower order terms more often. Technically, one should weight each term roughly as $(J_c/J_z)^o$, where o is the order at which the term appears in perturbation theory. We found it simpler, however, to use a conservative ratio of 5 between terms of different order. That is, for each 100 simulations, we sample Δ_{123} and Δ_{456} 100 times, Δ_{13} and Δ_{46} 20 times, and ΔB 4 times.

As the terms of the new basis are linear compositions of the B_n terms, the random variable associated with each term will differ from the underlying local field fluctuations. In particular, if each $B_n \sim \mathcal{N}(B_0, \sigma_B^2)$, then the relevant terms of new basis will be sampled from the distributions:

$$\begin{aligned} \Delta_{ijk} &\sim \mathcal{N}(0, 4\sigma_B^2) \\ \Delta_{ij} &\sim \mathcal{N}(0, 2\sigma_B^2) \\ \Delta B &\sim \mathcal{N}(0, 2\sigma_B^2) \end{aligned}$$

Supplementary E: Cross-Coupling

Perturbation theory provides the insight that beyond first order the Overhauser field cross-couples with charge noise in J_c at second order and above. This allows the Overhauser field to contribute non-trivially to two-qubit phases. For example, the two-qubit phase accumulation rate to second order for the butterfly configuration is given by:

$$\begin{aligned} J_{zz} &= \frac{1}{9} J_c + J_c^2 \frac{8(J_z^A + J_z^B)^2 - 5J_z^A J_z^B}{243 J_z^A J_z^B (J_z^A + J_z^B)} \\ &\star - \frac{2}{81} J_c \left(\frac{\Delta_{123}}{J_z^A} + \frac{\Delta_{456}}{J_z^B} \right) \\ &+ \mathcal{O}(J_c \Delta^2) + \mathcal{O}(J_c^2 \Delta) + \mathcal{O}(J_c^3), \end{aligned}$$

where $\Delta_{ijk} = B_i - 2B_j + B_k$, and where the coloured and starred line is the effect of cross-coupling. The intuition is that as J_c/J_z and the σ_B increase, the greater the two-qubit cross-coupling error. For the useful range of J_c/J_z values, and the experimentally inspired values of σ_B used in the main text, the effect of this cross-coupling is negligible.